Baseline Acoustic Levels of the EESC-USP Fan Rig

Bernardo Martinez R. Junior* and Paulo C. Greco Junior†
University of São Paulo, São Carlos, 13566-590, Brazil

Luciano C. Caldas‡ and Luiz A. Baccalá §
University of São Paulo, São Paulo, 05508-010, Brazil

Rafael G. Cuenca¶
Federal University of Santa Catarina, Santa Catarina, 89218-035, Brazil

Rudner Lauterjung Q.‖
Embraer S/A, São Jose dos Campos, 12227-901, Brazil

The EESC-USP Fan Rig is a long-duct low-speed experimental setup recently built at the Department of Aeronautical Engineering of the University of São Paulo. The objective is to provide a facility for studying fan aeroacoustics with a flexible configuration that allows changes in operational conditions of the rig. A parametric campaign was carried out exploring the effects of fan rotational speed, fan loading and rotor-stator spacing. Acoustic measurements were taken using an array of 77 wall-mounted microphones to provide a baseline data set for future comparisons. Hereby, data was processed to obtain the modal decomposition and power spectrum for each configuration. The last proved useful to compare tonal and broadband noise for each configuration. Experimental results indicate that changes in fan rotational speed scale noise generation mechanisms proportionally, do not affect noise spectral shape, and in consequence, are not useful to distinguish noise mechanisms. Although throttling does not seem to exhibit a clear effect on fan noise, it turns out that it is a good approach for cross-comparisons of other parameters' effect on fan noise, because of its direct modification on the flow structure within the duct. Results also showed that increasing rotor-stator spacing reduces both blade passing frequencies tone levels and the acoustic power of the interaction modes, which are in agreement with results obtained by similar test facilities.

Nomenclature

β^2	$1 - M^2$
$\mathbf{P}_{m,n}$	Modal power amplitude
ρ_0	Air density
σ	Hub-to-tip ratio
ζ	Cut-off frequency ratio
a	Duct radius
$b_{m,n}$	(m,n) Modal beamforming map
BPF	Blade passing frequency
C	Cross Spectral Matrix
c_0	Sound speed
f	Frequency
g	Steering vector
ICD	Inlet control device
J	Fan advance ratio
$J_m(x)$	Bessel function of first kind of order m
k_z	Axial wave number
$k_{m,n}$	Mode eigenvalue
m, n	Circumferential and radial mode orders
M_a, M_t	Axial and blade-tip Mach number
N	Number of microphones
$N_{m,n}$	Mode power normalization
$P_{m,n}$	(m,n) Modal pressure amplitude
r	Radial coordinate
RSS	Rotor-stator spacing

*Masters Student, Department of Aeronautical Engineering, bernardo.rocamora@usp.br, AIAA Student Member.
†Associate Professor, Department of Aeronautical Engineering, pgreco@usp.br, AIAA Member.
‡Research Engineer, lucianocaldas@usp.br.
§Professor, Department of Electrical Engineering, baccala@lcs.poli.usp.br.
¶Assistant Professor, rafael.cuenca@ufsc.br.
‖Collaborator Engineer, Aeroacoustics Division

I. Introduction

Aircraft noise is a major concern of the aeronautical regulators, since it is one of the most detrimental environmental effect of aviation. Besides obvious annoyance, it can bring many other problems for the communities near busiest airports as sleeping disorders, adverse academic performance of children, and possibly increased risk of cardiovascular diseases. Furthermore, this is a clear limit to traffic growth on these airports. In order to deal with this problem, ICAO has developed a strategy, the Balanced Approach to Aircraft Noise Management, to deal with multiple fronts of possible solutions, called pillars. One of its four pillars is the reduction of noise at source and its objective is to ensure the incorporation of latest available noise reduction technology into aircraft design. Aeroacoustics, the science of understanding of the phenomena generating noise in aircrafts, is an imperative field to the development of these new technologies, and, recently, an effort has been done to reduce the noise generated by the fan at the inlet and outlet of turbofan engines.

The Department of Aeronautical Engineering of the School of Engineering of São Carlos (University of São Paulo), in a joint venture with other Brazilian universities and Embraer S.A., has been involved in a research project called SILENCE that aims at understanding fan generated noise and developing new technologies to mitigate this issue. This project is divided in teams by subareas, as Fan Noise, Airframe Noise, and Liners Technologies. The authors have been involved with the understanding of Fan Noise and have been developing an experimental setup to investigate subsonic fan noise, the EESC-USP Fan Rig.

Subsonic fan noise can be generated by several aerodynamic phenomena: inflow disturbances, inlet/casing boundary layer, potential field interactions, and rotor-stator interaction; and even these phenomena could be subdivided. In order to go deeper in these topics, a parametric campaign of experiments was carried out at the current fan rig to isolate noise sources acting on a fan. Two main purposes motivate this work: state the baseline measurements of the NASA's Active Noise Control Fan (ANCF)[1] scaled fan geometry reproduced at the current rig setup and, similarly to what has been done in the DLR low-speed fan rig,[2] characterize and quantify the effects of rotational speed, rotor-stator spacing (RSS), and loading on fan generated noise. That was an opportunity to characterize and quantify the setup so that when new configurations are available, this baseline results could be used for comparison.

This paper is organized as follows: Section II talks briefly about the experimental setup, in which the rig, its capabilities and its instrumentation are described, Section III shows the signal processing techniques used, where the methods for analyzing the experimental data collected are described, Section IV presents the results obtained from the parametric campaign with discussion. The paper ends with a brief conclusion section and an appendix with the complementary data not exposed throughout the text.

II. Experimental Setup

The current EESC-USP Fan Rig configuration, a long-duct low-speed fan rig inspired on DLR's test facility, depicted in Figure 1, is composed by a duct about ten meters long with its axis positioned 1.3 m above the floor over a metallic workbench. The duct radius at the inlet and the outlet has a diameter of 0.6 m, and at the fan-stator stage there is a contraction to a diameter of 0.5 m, which was done aiming the reduction of the casing boundary layer. At the inlet there is a glass-fiber bell-mouth installed, with an axisymmetric elliptic curvature geometry decreasing from 1.36 m to 0.6 m, this provides a smoother air inflow, avoids separation and reduces non-uniformities entering the duct. The outlet has an anechoic termination with the purpose of mitigating the abrupt change in acoustic impedance for the exiting flow. Each of this device chambers work as a resonator, attenuating some frequency bands and, overall, the device reduces the sound wave reflections at the exhaust back to the duct. Its design is based on the Annex E of the ISO 5136 standard. The ducts are installed close to the ground and the ingested air is influenced by the turbulence level, which is different to what is found in higher altitudes (condition of aircraft flight), and by the asymmetries generated by the proximity to a wall (the ground floor), like the alteration on the potential flow and the appearance of a ground vortex. These flow distortions are believed to have a significant effect on the noise and bring the fan away from flight condition. The Inlet Control Device (ICD) is located at the duct inlet where an elliptical bell-mouth is installed. It is a dome-shaped structure, inspired on that described by Homyak,[3] but, for now, with the main the objective being achieving a turbulence reduction, we are only using a steel wire mesh, with a porosity of about 60%.

The fan diameter is 0.5 m and it is composed by a 16-bladed rotor and a 14-vaned stator, and their

Figure 1. *Left:* **Current EESC-USP Fan Rig setup.** *Right:* **16-bladed fan close up.**

geometry reproduce the one from NASA's ANCF. It is driven by a Remy HVH-250-115 DOM 100 hp electrical motor which is mounted inside the duct, supported by three struts, and is capable of reaching speeds up to 4500 rpm, producing axial flows up to Mach 0.14 and tip speeds of around Mach 0.37. The Reynolds number relative to the rotor tip chord and speed range about 10% around 400,000.

II.A. Instrumentation

There are two main instrumentation systems on the EESC-USP Fan Rig: one of simultaneously high acquisition frequency that accounts the acoustic measurements, and one for low acquisition frequency which is responsible for the pressure, vibration and safety measurements. The high frequency system has the acoustic measurements carried out with G.R.A.S. 40PH-S2 ϕ7 mm and B&K Type 4958 ϕ7 mm microphones. These are microphones with great accuracy in phase match and frequency bandwidth from 20 Hz to 20 kHz, therefore being ideal to the fan noise measurements.

The acquisition is done using a NI PXI-1042Q chassis, and NI 4496 and NI 4498 module boards. They are connected to a computer via optical fiber (due to the high acquisition frequency) and the acquisition software was developed by Federal University of Santa Catarina, in Brazil. Aiming the determination of the sound power radiated across the duct, an arrangement of flush-mounted microphones is set: an array of three rings, with 33, 23 and 21 equally distributed microphones in each ring. The first ring, with 33 microphones, is at an spacing of 0.70 m upstream from the fan, the next is away 0.10 m from the first and the third is 0.17 m away from the second. Also, the signal obtained with a hall sensor is acquired using this system.

The second acquisition system used is the NI cDAQ-9184. Static pressure is measured in several positions: at the inlet, before the fan, between fan and stator, after stator and at the outlet; dynamic pressure is measured at the inlet and the outlet; and vibration is measured with accelerometers installed at the stator and the motor bedding. The cDAQ is connected to a PC via Ethernet and the acquisition is done using Matlab and Labview. These are used for performance measurements, i.e. determination of fan pressure rise, fan efficiency and mass flow rate.

Finally, ambient temperature, pressure and humidity are measured using a meteorological station installed at the hangar. This data is used to correct the other measurements and obtain parameters as the air density.

II.B. Parameters variations and test matrix

Three main parameters were analyzed in the present work: fan rotational speed, fan loading, and rotor-stator spacing. Fan speed is set by a software that controls the electrical motor inverter. The constraints are a 30A maximum current and 5000 rpm. Here we chose to work with speeds from 3500 rpm to 4500 rpm, with a 250 rpm step. This maximum speed was the one in which we still observed acceptable levels of vibration. Interchangeable screens with different area restrictions compared to the open outlet (600 mm diameter duct) were fabricated to control fan loading, a throttling device was installed at the duct exhaust, which rejects the flow to the hangar outside, open ambient. This area restrictions have an effect on the axial speed of the flow and changes the angle of attack of the rotor blades. For this device fabrication, the international standard ISO 5136 recommendations were used, with some small modifications. The fabricated screen area

restrictions were: 0.0% (no screen), 24.3%, 37.7%, 52.2%, 63.0%, 74.7%., but, for sake of simplification, these screen areas are marked on the plots below as 0%, 25%, 40%, 50%, 60%, 70%. Finally, rotor-stator spacing was changed by increasing shaft and hub length between rotor and stator. In chord spacing, here defined as the mean distance between rotor blade trailing edge and the vanes leading edge, divided by the rotor blade mean chord, three configurations were designed: 0.43, 0.95, and 1.5. All three configurations are to be tested, but at the current time only the first two configurations were extensively tested.

Table 1 enumerates the tests conduced and presented in this paper. Conditions 1, 2 and 3

Table 1. Test matrix

Parameter	RSS	Inflow	Throttling	RPM	Parameter	RSS	Inflow	Throttling	RPM
Condition 1	0.43	ICD	0%	4250	Condition 11	0.43	ICD	0%	3750
Condition 2	0.95	ICD	0%	4250	Condition 12	0.43	ICD	0%	3500
Condition 3	1.50	ICD	0%	4250	Condition 13	0.95	ICD	0%	4500
Condition 4	0.43	ICD	25%	4250	Condition 14	0.95	ICD	0%	4000
Condition 5	0.43	ICD	40%	4250	Condition 15	0.95	ICD	0%	3750
Condition 6	0.43	ICD	50%	4250	Condition 16	0.95	ICD	0%	3500
Condition 7	0.95	ICD	60%	4250	Condition 17	0.95	ICD	25%	4250
Condition 8	0.95	ICD	70%	4500	Condition 18	0.95	ICD	40%	4250
Condition 9	0.43	ICD	0%	4500	Condition 19	0.95	ICD	60%	4250
Condition 10	0.43	ICD	0%	4000	Condition 20	1.50	ICD	40%	4250

III. Data Post-Processing Techniques

III.A. Spectral analysis

A standard way to characterize aeroacoustic measurements is throughout their power spectral density. As input, for each configuration, a sampling frequency of 51.2 kHz and 39 seconds of acquired acoustic data is used, which allows the adequate use of the well-known Welch's method[4,5] with 2048 samples Hanning window and 50% overlap. Plots are displayed in terms of SPL levels by taking the logarithmic value with reference to $p_{ref} = 20\mu Pa$ sound pressure, i.e., $SPL = 10 \cdot log_{10}(S/p_{ref}^2)$, where S is the power spectrum density estimated.

III.B. Modal analysis

A special characteristic of fan generated noise is the possibility, when it is inserted in a duct of constant cross section with constant boundary conditions (as a hard wall casing) and medium (incompressible air), to obtain a series expansion of the wave equation solution for time-harmonic perturbations. Each of these self-similar solutions is called a mode. These modes are important because their a simple way to represent very complex solutions of the acoustic field and they can be used to identify noise generation mechanisms.

Modal decomposition here is obtained using beamforming, which is a well-used technique for locating noise sources for a range of desirable frequencies.[5] To achieve this task an array of microphones was specially designed for this setup, taking as input requirements: the signal bandwidth, focal distance, duct diameter, blade and vane counting and the maximum circumferential order of modes we desire to measure. The blade and vane counting and the maximum mode order are directly related through Tyler-Sofrin[6] relation, which states the limits of cut-on duct modes. The amount of sensors in each ring accounts for the maximum circumferential order detectable. As for the maximum radial order, there is a need for multiple rings of sensors.

The classical beamforming formulation used in this work is nearly the same as described by Caldas *et al.*[7,8] as follows

$$b_{m,n} = \frac{g_{m,n} \cdot C \cdot g_{m,n}^H}{\sqrt{N \|g_{m,n}\| \|g_{m,n}\|^H}} \tag{1}$$

where C is the cross-spectral matrix and $g_{m,n}$ is the modal steering vector computed mode by mode. The main diagonal of C is excluded to avoid boundary layer noise in the auto-spectra of each sensor.[5] The square root added in the denominator of Eq. 1 was empirically tested and led to a better results in terms of modal power levels. Dougherty[9] showed that a slight weight modification in the formulation 1 would lead results proportional to acoustic pressure, instead of source power. This is obtained by

$$b_{m,n} = \frac{\|g_{m,n}\|\|g_{m,n}\|^H}{N} b_{m,n} \tag{2}$$

The steering vector formulation used is given by

$$g_{m,n}(\vec{r_i}, \vec{r_s}, \omega) = \frac{J_m(k_{m,n} r_i) J_m(k_{m,n} r_s)}{N_{m,n}^2} e^{jm(\theta_i - \theta_s)} e^{-jk_z^{(-)}(z_i - z_s)} \tag{3}$$

where $J_m(x)$ is a Bessel function of first kind, $\vec{r} = (r, \theta, z)$ is the position vector in cylindrical coordinates, subscripts i and s refer to microphone and mesh point indexes, respectively. $k_z^{(-)}$ is the axial wave number. The up-script $^{(-)}$ means the upstream propagation wave, i.e., from the fan to the microphone array. Values of $k_{m,n}$ are computed so that $J'_m(k_{m,n}a) = 0$, i.e., the product $k_{m,n}a$ is the n^{th} stationary point of order m of the first kind Bessel function $J_m(x)$. $N_{m,n}^2$ in Eq. 3 is a mode normalization for energy conservation, it is computed by

$$N_{m,n}^2 = \left(1 - \frac{m^2}{(k_{m,n}a)^2}\right)^2 \tag{4}$$

In order to obtain sound pressure (or amplitude) of each (m,n) mode, the output beamforming map $b_{m,n}$ should be integrated over the duct cross section $\mathbf{S}$. This can be achieved by

$$P_{m,n}^2 = \int_{\mathbf{S}} b_{m,n} d\mathbf{S} \tag{5}$$

where $P_{m,n}^2$ is the estimated pressure amplitude of the respective (m,n) mode. However, a suitable representation for modal analysis relies on their respective power level (PWL) $\hat{\mathbf{P}}_{m,n}$ instead of SPL levels. Hopefully, the mode power can easily be obtained from the pressure level by the formulation introduced by Sutliff[10]

$$\hat{\mathbf{P}}_{m,n} = \mp \frac{\pi a^2 (1 - \sigma^2)}{\rho_0 c_0} \beta^4 Re\left\{ \frac{\sqrt{1 - \frac{1}{\zeta^2}}}{\left\|1 \pm M\sqrt{1 - \frac{1}{\zeta^2}}\right\|^2} \right\} \|P_{m,n}^2\| \tag{6}$$

where

$$\zeta = \frac{f}{f_c} = \frac{2\pi f}{c_0 \beta k_{m,n}},$$

$\beta^2 = 1 - M^2$ and ζ is the cut-off ratio as defined by Sutliff,[10] i.e., the ratio between the frequency of interest and the cut-off frequency for the given (m,n) mode order. In the special case of $k_{m,n} = 0$ (or 'infinite' axial wave number) defines the cut-off frequency f_c. Indeed, the eigenvalue $k_{m,n}$ increases with m or n and f_c also increases for higher order modes.

IV. Results and Discussion

This section is organized into four subsections: IV.A, in which a compilation of the flow measurements and calculated flow structure is presented, IV.B, in which spectral and modal analysis are done for multiple fan speed, IV.C, in which spectral and modal analysis are done for multiple throttling configurations, and IV.D, in which spectral and modal analysis are done for multiple rotor-stator spacings.

IV.A. Flow measurements

Table 2 contains flow measurement values for the test conditions presented above flow measurements at the EESC-USP Fan Rig include steady static pressure taps at the inlet (denoted $p_{st,1}$), one chord upstream to the fan blade leading edge ($p_{st,2}$), between fan and stator ($p_{st,3}$) and one chord downstream to stator vane trailing edge ($p_{st,4}$), Pitot-static measurement at the inlet (from which M_{inlet} and M_{axial} are calculated). This table also contain air density from each test condition calculated from ambient pressure and humidity. These two were obtained for each test, but their values are suppressed here. Also, from rotational speed and calculated axial velocity, it was possible to calculate advance ratio, J, the angle of attack at the hub and the tip of the blades and the Reynolds number at blade tip, using the blade tip velocity and chord.

Figure 2(a) shows the dependency of the Mach number with the rotational speed of the fan. As expected, the increase in rotational speed increases both axial and tangential Mach numbers. These increases self compensate and the resultant advance ratio, maintaining the same throttling, remains constant. Another interesting feature, both present in Figure 2(a) and Figures 2(b) and Figure 2(c) is the fact that changing the rotor-stator spacing does not affect the aerodynamic performance of the fan. Figures 2(b) and Figure 2(c) also show the decrease of the static pressure relative to ambient pressure with the increase in fan speed.

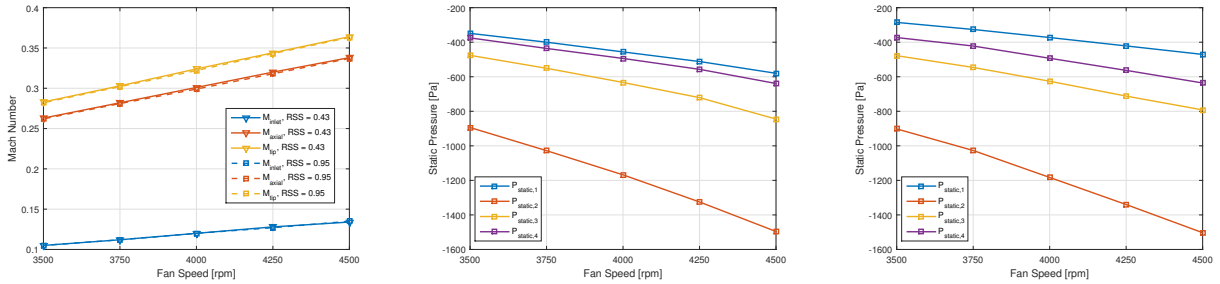

(a) Mach number vs. fan speed (RSS = 0.43 and 0.95)

(b) Static pressure along the duct *vs.* fan speed (RSS = 0.43).

(c) Static pressure along the duct *vs.* fan speed (RSS = 0.95).

Figure 2. Duct flow characteristics changing with the rotational speed of the fan.

Figure 3(a) shows the dependency of the advance ratio with the area restriction at the duct outlet. Different to changes in rotational speed, the increase in area restriction alters the flow structure, represented here by the reduction on the advance ratio, J. Figures 3(b) and 3(c) show the static pressure along the duct due to changes in throttling, all ports show the increase in static pressure with more throttling, but the static ports after the fan show positive static pressures, due to the great pressure rise caused by the fan with higher loading.

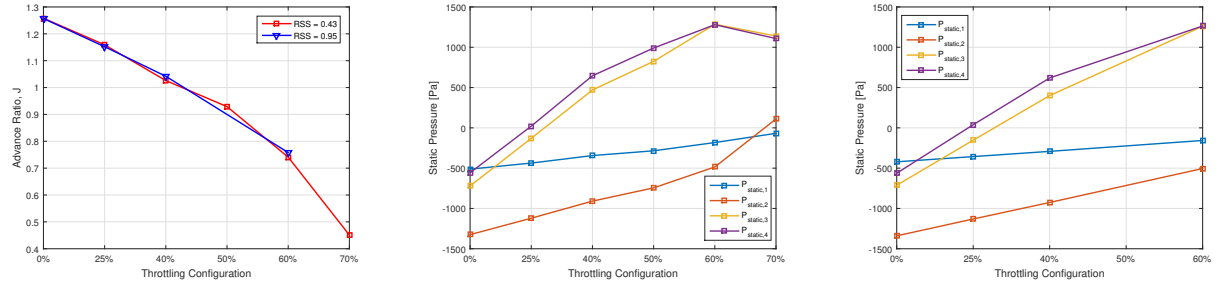

(a) Advance ratio vs. throttling

(b) Static pressure along the duct *vs.* fan speed (RSS = 0.43).

(c) Static pressure along the duct *vs.* fan speed (RSS = 0.95).

Figure 3. Duct flow characteristics changing with throttling.

IV.B. Effects of rotational speed

As it is possible to see at Table 2, the fan advance ratio and blade angle of attack maintain themselves constant as the fan rotational speed is increased. That happens because, for a given loading condition, the aerodynamic flow structure adjusts itself to the fan speed. As stated by Moreau and Enghardt,[2] in this

case, the noise sources scale similarly to each other, and a increase throughout the whole frequency spectra is expected, conserving its shape. Conditions 9, 1, 10, 11, 12, and conditions 13, 2, 14, 15, 16 explore this effect for rotor-stator spacing of 0.43 and 0.95, respectively.

The first set results (conditions 9, 1, 10, 11, 12) are presented in Figure 4 below. First graph shows the relation between the noise spectra and shaft speed, where, overall, the shape of the spectra is unaltered by the increase in rotational speed. There are, however, some perceivable exceptions, as, for example, the appearance of a tone at frequencies lower than the first BPF tone for the higher speeds. The increase in the first BPF seems to be linear with the rotational speed, but the following ones do not have a straightforward pattern. Broadband noise levels are increased quite consistently with the speed, including the high frequency bubble, that appears at this fan loading. Conditions 13, 2, 14, 15, 16, are shown in Figure 14 at the appendices.

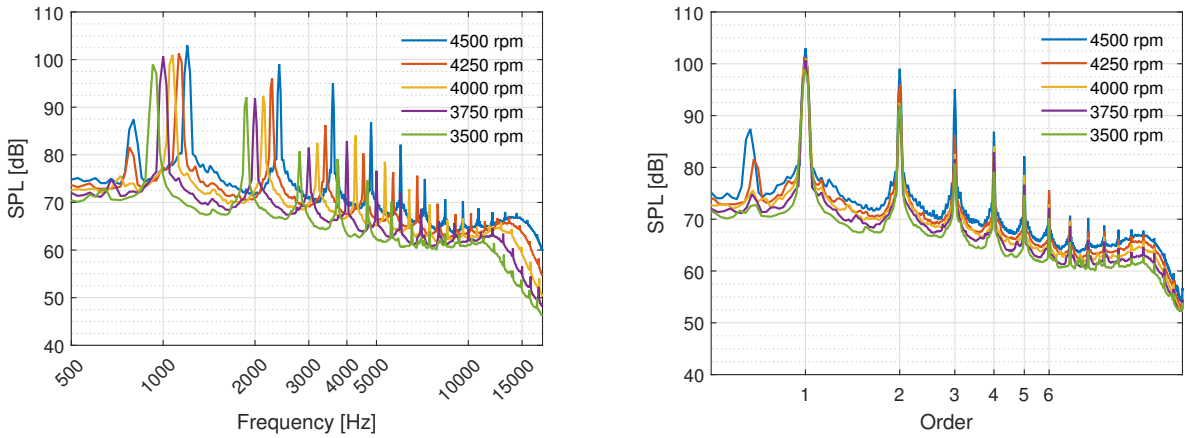

(a) on frequency domain.

(b) on shaft order domain.

Figure 4. Average spectra comparing multiple rotational speeds (RSS = 0.43 and open throttle).

Figure 5(a) shows the variation on the broadband level in a comparison to the higher rotational speed,5(b) a comparison to the rotational speed 250rpm above it, and 5(c), the results of the integration between some frequency bands (low frequency band, from 500 Hz and 2 kHz; high frequency band, from 2 kHz and 7 kHz; overall frequency, from 500 Hz to 7 kHz; and bubble frequency band, from 7 kHz to 15 kHz). The overlap in the curves in 5(b) and results of the integration shown in 5(c) confirm that the additional broadband (in dB) can be considered linear with the variation in fan speed for the given conditions, and this apply throughout the whole spectra. Additionally, the result of the integration shows that there is as much energy on broadband noise for the lower and the higher frequency bands.

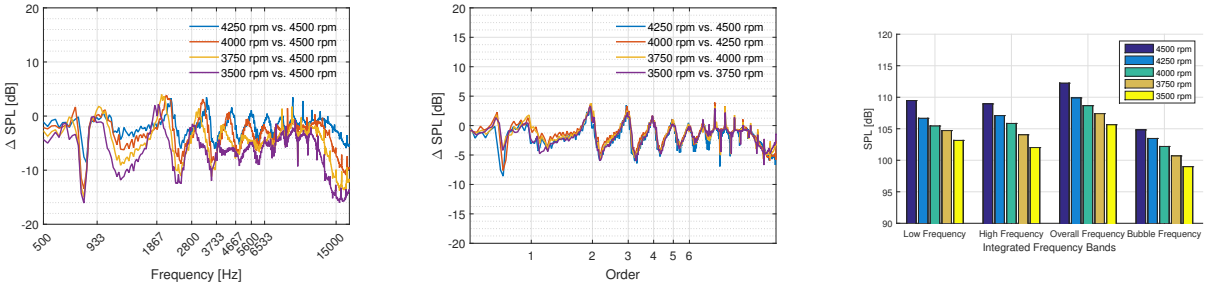

(a) Variation on SPL level (on frequency domain).

(b) Variation on SPL level (on shaft order domain).

(c) Integration of broadband noise.

Figure 5. Analysis of the effect of RPM on broadband noise (RSS = 0.43 and open throttle).

In Figure 6, it can be seen that the summation of the first six BPFs tone levels (called here overtone) is monotonically increasing on an average of 1dB with an increase of 250 rpm on fan speed. However, when we analyze the BPFs one by one, the relation has no clear pattern on their variation. The first two BPFs

follow the same behavior of the overtone, the 3rd grows at higher rates each time the fan speed is raised and the last three have eventual reductions.

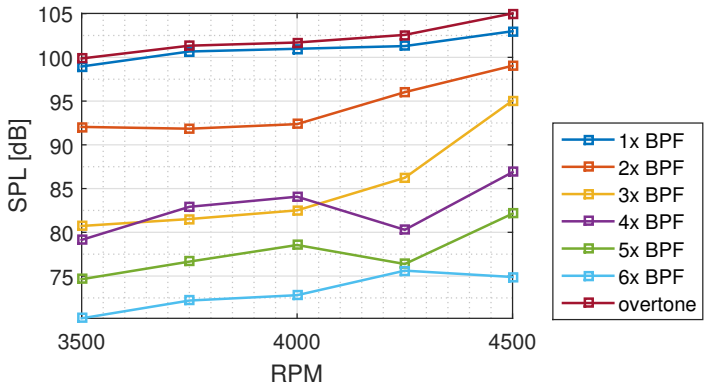

Figure 6. Analysis of the BPFs tone levels and overtone (their sum) (RSS = 0.43 and open throttle).

The rotational speed has a clear effect on the Tyler-Sofrin modes. Reducing the fan speed, directly reduces the SPW of these rotor-stator interaction modes as it can be seen for the (2,0) mode in Figure 15, and for the (4,0) and (6,0) modes at the 2nd and 3rd BPFs, respectively, as shown in Figure 16 and 17. It is also relevant to point out that these modes are fully dominant at the 1st (Figure 15) and 2nd BPFs (Figure 16), with at least 20dB over almost all other cut-on modes, but this beyond the 3rd BPF, this no longer applies and the modal structure, besides still being dominated by the interaction mode, also has other relevant components (Figure 17). Figure 23 compiles the effect of the rotational speed on (2,0), (4,0) and (6,0) interaction modes PWL values. Its is possible to see that, for both, rotor-stator spacings, the tendency is of an increase on the PWL value, just as seen with the BPF tone levels.

IV.C. Effects of throttling

By changing screens at the duct outlet, we were able to change the flow condition of the fan. The throttling device affects the mass-flow inside the duct and, since the angle of attack of the fan blades is given both by axial and tangential velocity, increasing the area restriction on the duct outlet we induce an increase in fan loading. Only the first five throttling screens were utilized, up to a 70% of area restriction. Beyond that, the fan was already stalled and no further tests were of interest. Conditions 1, 4, 5, 6, 7 and 8, conditions 2, 17, 18 and 19, and conditions 3 and 20, explore this effect for RSS = 0.43, RSS = 0.95, and RSS = 1.50, respectively.

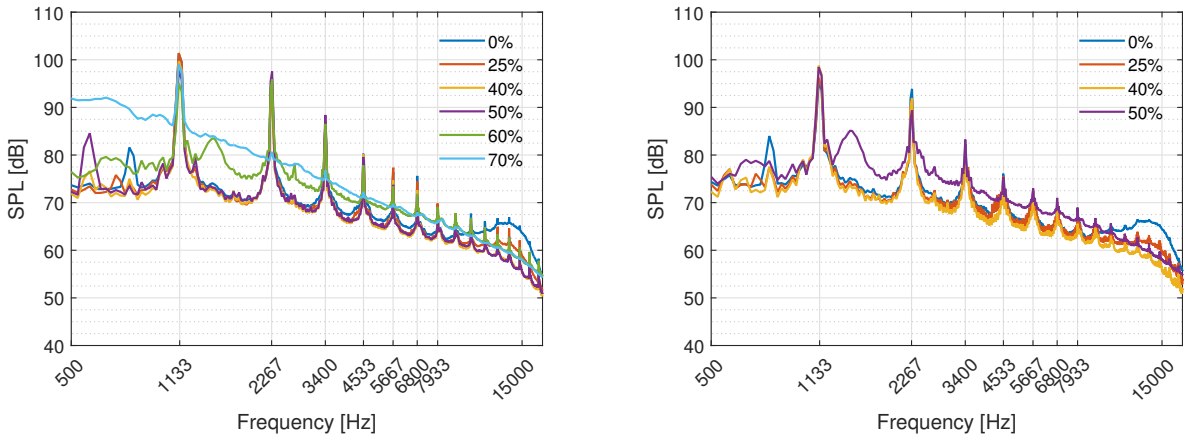

(a) RSS = 0.43.

(b) RSS = 0.95.

Figure 7. Averaged spectra for multiple throttling configurations and fan speed of 4250 rpm.

Figure 7, shows the averaged spectra for different loading conditions and two different rotor-stator spacings. It is worth mention that the fan noise becomes highly broadband for higher area restriction (>50% of the duct area). The reason for this, probably, is that the fan blades are already in stall condition, because of the blades' angle of attack increase. In this condition, the fan pumps fewer air each time (the axial speed becomes smaller with the increase in area restriction - see Table 2), and the blade wakes are larger and more turbulent. The stalled condition does not necessarily need to affect the whole fan and does not change the fact that while there is still axial flow, there is pressure oscillation due to fan wakes on the stator vanes. But curiously enough, when the area restriction reach 70%, only the 1st BPF is still present. Another effect is the relation with the high frequency bubble: this decrease in axial speed caused by throttling makes the bubble weaker and even disappear for area restrictions higher than 40%. When analyzing the broadband (Figure 8(a)), compared to the open throttle, the other non-stalled configurations, apart from the bubble frequencies, are altered by less than 2dB, but when compared to consecutive conditions, it is possible to see that reduction comes from the 0% to 25% configuration, from 25% not much changes and from 40% to 50%, there is an actual increase in broadband level. Integration of the broadband spectra (Figure 8(b)) confirms this behavior and shows that this increase in broadband can lead to a very noisy fan.

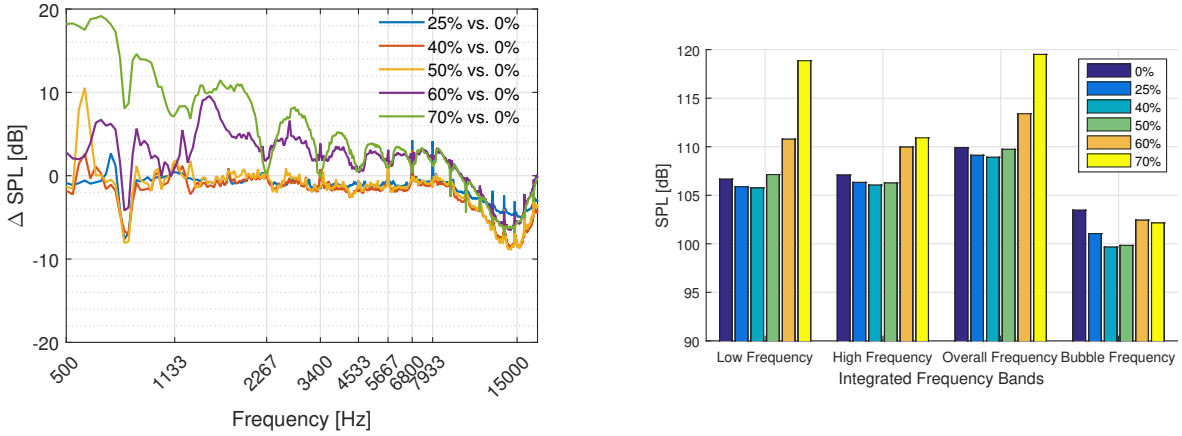

(a) Variation on SPL level (on frequency domain).

(b) Integration of broadband noise.

Figure 8. Analysis of the effect of throttling on broadband noise (RSS = 0.43 and open throttle).

When analyzing the BPF tone levels (Figure 9), the overall behavior for the non-stalled configurations is a small reduction on its value, another curious behavior happens with the second BPF, which seems to increase by the same amount that the 1st BPF is reduced from 25% to 50% area restriction.

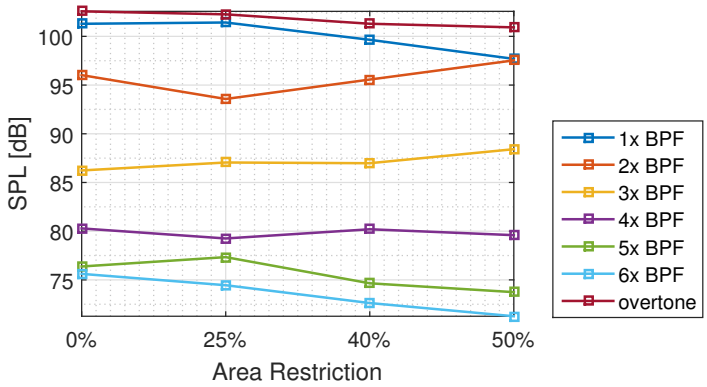

Figure 9. Analysis of the BPFs tone levels and overtone (their sum) (RSS = 0.43 and 4250 rpm).

Figures 18, 19 and 20 present the comparisons for different throttle conditions with respect to the first three BPFs. It is possible to see that the modal structure is clearer at lower loadings and the interaction modes (2,0), (4,0), (4,1), (6,0), (6,1), (6,2) are prominent. Figure 21 was taken at the center frequency of the

bubble that appear on the spectra of lower loading configurations. In it we try to observe what could be the reason for its existence. Some negative m-modes near the cut-off area show high values at these lower loading configurations and these modes lose power as the loading is increased. But more detailed investigation on the frequencies composing the bubble is needed to confirm this hypothesis.

Figures 24 and 25 compile the effect of the decrease in axial speed induced by imposing an area restriction on the duct outlet on (2,0), (4,0) and (6,0) interaction modes PWL values. Its is possible to see that, for both, rotor-stator spacings, and before stalling, there is not a direct effect on the PWL values that can be spotted.

IV.D. Effects of rotor-stator spacing

From the current beliefs, we expect subsonic fans to have cut-off rotor-alone noise and most of the noise coming from the rotor-stator interaction. This interaction have many noise generating mechanisms itself, but the impingement of the blade wakes on the stator vanes are believed to account for most of this generation. Therefore, bringing the fan downstream, i.e. increasing the gap between rotor blades and stator vanes, would affect tonal noise, that because, with the spacing, the blade wakes are exponentially smoothed out before hitting the stator vanes. Figure 10 shows the effect on the averaged spectra and, as expected, the reduction on the BPF tone levels. It is also interesting noticing that, as explained by Goldstein,[11] the higher order BPF tones intensities are preferably reduced, since it is possible to represent the pressure fluctuations with less components when the deficit in velocity on the blade wakes are smoothed out. Broadband noise is also affected. In our experiments, as the tone levels are reduced, the broadband is increased, as it is possible to see in Figure 10.

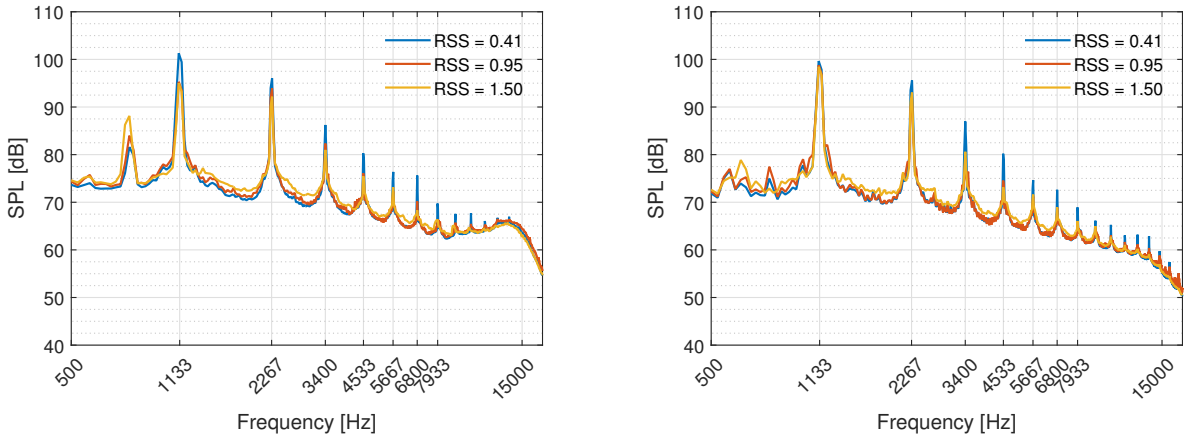

(a) Open throttle.

(b) Throttle at 40%.

Figure 10. Averaged spectra for multiple rotor-stator spacing configurations and fan speed of 4250 rpm.

Figure 11 explore the effect of rotor-stator spacing on the broadband SPL levels. It is possible to see in 11(a), up to the 2nd BPF, broadband is increased at least 0.5 dB (up to 2.5 dB) and then this increase is almost zero up to the bubble frequencies, were, one again, broadband is increased to higher levels. Figure 11(b) shows the integration of the spectra broadband for the three RSS. Again, it is possible to see that there is a increase throughout both low and high frequency bands, but the increase at the low frequency band is bigger.

Figure 12(a) is the variation between different configurations of RSS and its data has too much noise to find behavior. Figure 12(b) contains the filtered data of 12(a) (using a moving average filter with 20 samples), which confirm us as higher broadband level when the gap between rotor and stator is increase. Nevertheless, how much higher and at what frequency bands depend on the fan loading. Between the 1st and the 2nd BPF, the higher the loading the lower is the increase in broadband. But for higher frequencies, the higher increase in broadband is found for the 25%-throttling configuration.

The BPF tone levels for the three spacing configurations is seen in Figure 13(a). An overall decrease (also perceivable when the tone levels are added up, called overtone) is observed. The overtone goes from 102.5 dB to 97 dB when the spacing goes from 0.41 to 0.95. Figure 13(b) compares the effect of increasing

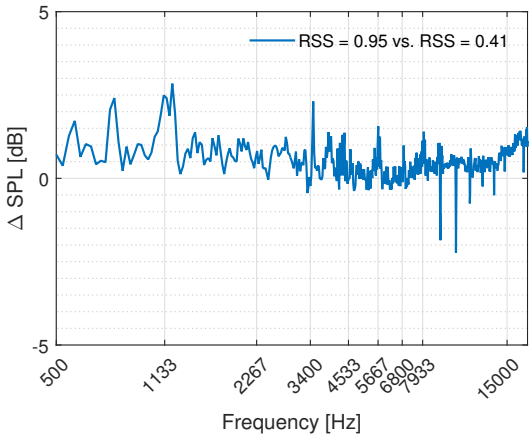

(a) Variation on SPL level (on frequency domain).

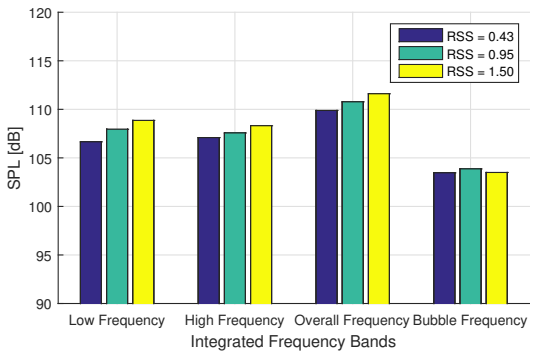

(b) Broadband noise integration.

Figure 11. Analysis of the effect of rotor-stator spacing on broadband noise for multiple throttle configurations.

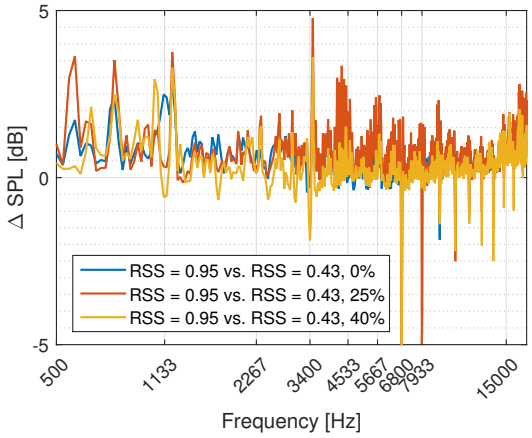

(a) Variation on SPL level (on frequency domain).

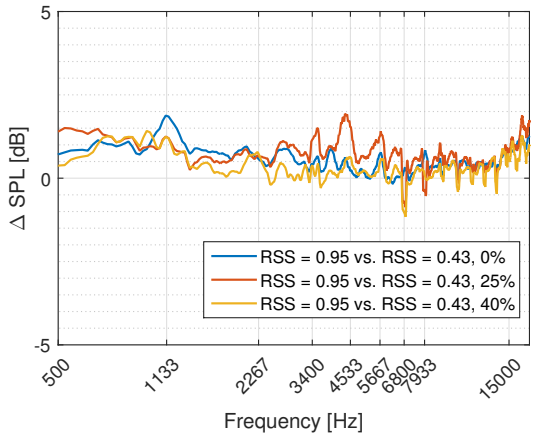

(b) Filtered variation on SPL level (on frequency domain).

Figure 12. Analysis of the effect of rotor-stator spacing on broadband noise for multiple throttle configurations.

the loading on the BPF tones reduction. The increase in loading reduces the axial speed, and, therefore, increases the distance travelled by the wakes of the blades. As the wakes have to cover a higher distance, they are more smoothed out and, higher decreases, are expected and in general, confirmed by Figure 13(b).

Figure 22 show modal decomposition for the first six BPFs for the 4250 rpm configuration. In general, the Tyler-Sofrin modes are dominant and the acoustic power of these modes is reduced with more spacing. This is more evident for the first and the higher order BPFs (as it is possible to see in Figure and Figure), nevertheless it is not always true for all the BPFs, as it is possible to see with the (8,0) mode for the 4^{th} BPF. Figure 26 compile the effect of the rotor-stator spacing on (2,0), (4,0) and (6,0) interaction modes PWL values, these modes power are, in general, decreased, as expected by the pattern on the BPFs.

V. Concluding Remarks

An effort to understand fan generated noise and its sources is being taken at the Department of Aeronautical Engineering at the University of São Paulo. From a parametric campaign taken at the EESC-USP Fan Rig, in which several fan speed, loading conditions, rotor-stator spacing and inflow configurations, noise spectral and modal components are presented. A good part of the expected effects, as the rotor-stator interaction modes at the blade passing frequencies, were observed, in agreement with literature and publications of other similar fan rigs. This experimental data collected at this parametric campaign will also be valuable

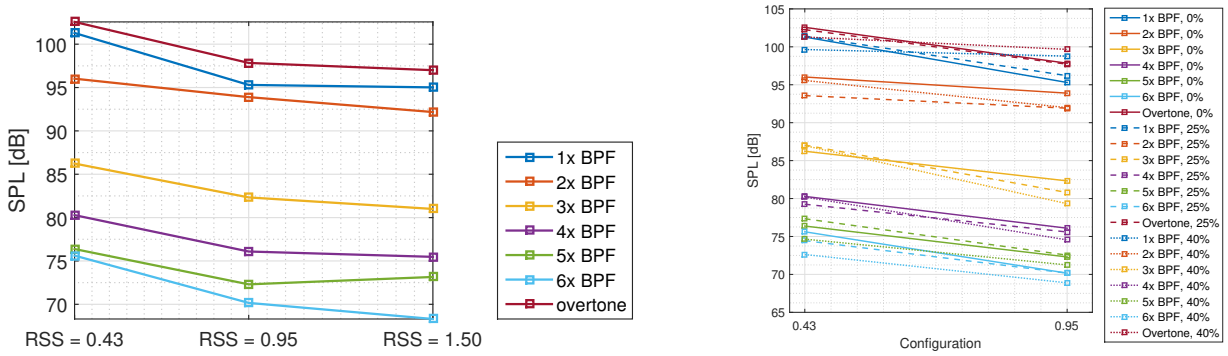

(a) Open throttle.

(b) Throttle from 0% to 40% area restriction.

Figure 13. Analysis of the BPFs tone levels and overtone (their sum) at 4250 rpm.

as input for semi-empirical and semi-analytical prediction methods which are developed at the University of São Paulo. Also, it will valuable for the development of noise reduction technologies in partnership with other Brazilian universities members of the SILENCE Project.

Improvements on the EESC-USP Fan Rig experimental setup are constantly being taken, next steps include the installation of instrumentation near the fan blades and stator vanes, in order to achieve a better characterization of the flow ingested by the fan and lead to a noise source separation. Casing boundary layer, ingested turbulence, velocity profile are parameters that, when measure, will bring a lot of knowledge about correlations.

Acknowledgments

The EESC-USP Fan Rig was financially supported by FINEP (Federal Founding for Development of Science and Research) and was designed, manufactured and assembled with the help of the technicians and engineers of the School of Engineering of São Carlos (USP) and with the EMBRAER's engineering team cooperation. This research started with Embraer's Silent Aircraft Project, and now keeps running with Embraer's SILENCE Project. The authors thank all involved in this project, including NASA Glenn Research Center staff, specially Daniel Sutliff, whose support and technical insight proved very helpful.

References

[1]Sutliff, D. L., Nallasamy, M., Heidelberg, L., and Elliott, D., "Baseline acoustic levels of the NASA active noise control fan rig," *AIAA paper*, 1996, pp. 96–1745.

[2]Moreau, A. and Enghardt, L., "Ranking of fan broadband noise sources based on an experimental parametric study," *15th AIAA/CEAS-2009-3222 Aeroacoustics Conference, Florida*, 2009.

[3]Homyak, L., McArdle, J., and Heidelberg, L., "A compact inflow control device for simulating flight fan noise," *AIAA Paper*, Vol. 83, 1983, pp. 0680.

[4]Percival, D. B. and Walden, A. T., *Spectral Analysis for Physical Applications*, Cambridge University Press, 1993.

[5]Mueller, T. J., *Aeroacoustic Measurements*, Springer, 2001.

[6]Tyler, J. M. and Sofrin, T. G., "Axial flow compressor noise studies," *Transactions of the society of automotive engineers*, Vol. 70, 1962, pp. 309–32.

[7]Caldas, L. C., Herold, G., Greco, P. C., and Baccala, L. A., "In-duct Rotating Beamforming and Mode Detection of Fan Noise Sources," *AIAA 2016-3034, 22st AIAA/CEAS Aeroacoustics Conference*, American Institute of Aeronautics and Astronautics, 2016.

[8]Caldas, L. C., *In-duct beamforming and mode detection using a circular microphone array for the characterisation of broadband aeroengine fan noise*, Master's thesis, Escola politécnica da Universidade de São Paulo, São Paulo, Brazil, 2016.

[9]Dougherty, R. P. and Walker, B. E., "Virtual Rotating Microphone Imaging of Broadband Fan Noise," *15th AIAA/CEAS Aeroacoustics Conference (30th AIAA Aeroacoustics Conference)*, American Institute of Aeronautics and Astronautics, 2009.

[10]Sutliff, D. L., "Rotating Rake Turbofan Duct Mode Measurement System," *International Journal of Aeroacoustics*, 2007.

[11]Goldstein, M. E., *Aeroacoustics*, Vol. 1, 1976.

Appendices

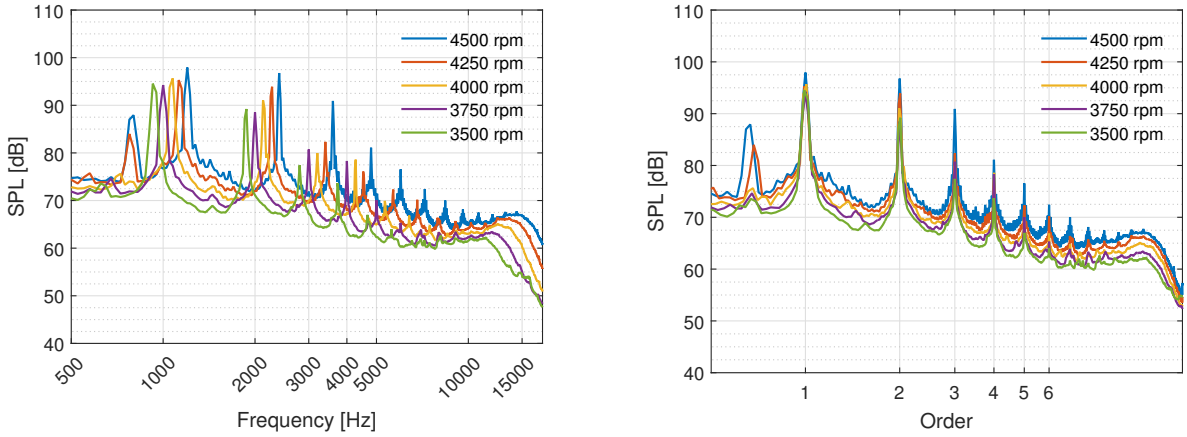

(a) on frequency domain.

(b) on shaft order domain.

Figure 14. Average spectra comparing multiple rotational speeds (RSS = 0.95 and open throttle).

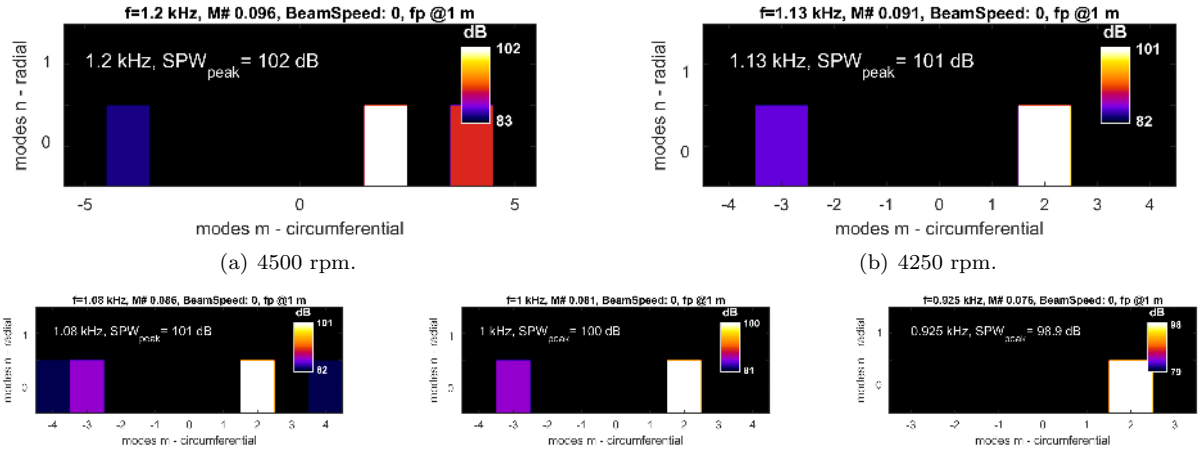

(a) 4500 rpm.

(b) 4250 rpm.

(c) 4000 rpm.

(d) 3750 rpm.

(e) 3500 rpm.

Figure 15. Modal decomposition of the 1st BPF for multiple fan rotational speeds (RSS = 0.43 and open throttle).

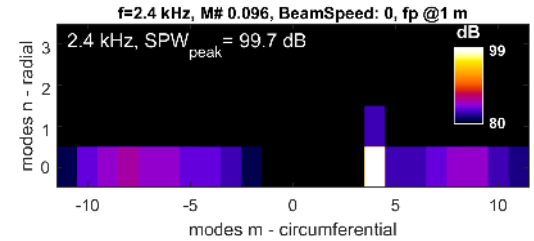

(a) 4500 rpm.

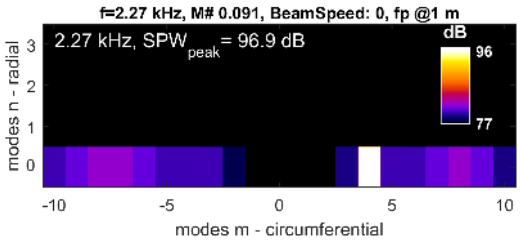

(b) 4250 rpm.

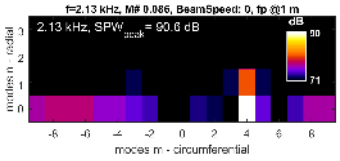

(c) 4000 rpm.

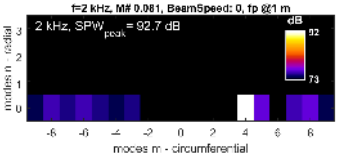

(d) 3750 rpm.

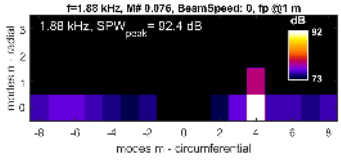

(e) 3500 rpm.

Figure 16. Modal decomposition of the 2nd BPF for multiple fan rotational speeds (RSS = 0.43 and open throttle).

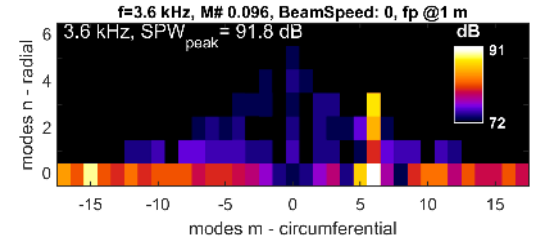

(a) 4500 rpm.

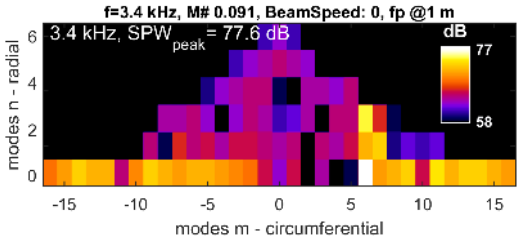

(b) 4250 rpm.

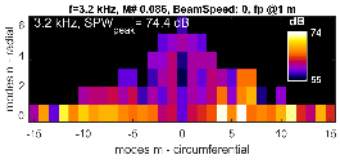

(c) 4000 rpm.

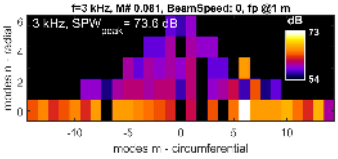

(d) 3750 rpm.

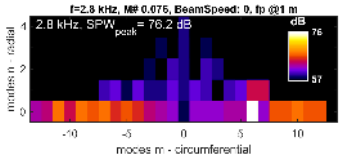

(e) 3500 rpm.

Figure 17. Modal decomposition of the 3rd BPF for multiple fan rotational speeds (RSS = 0.43 and open throttle).

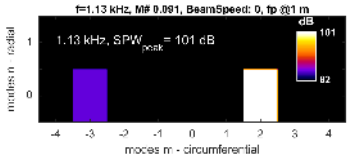

(a) Open throttle.

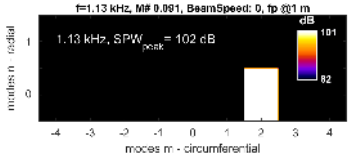

(b) Throttle at 25% of area restriction.

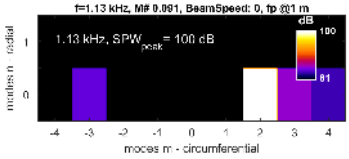

(c) Throttle at 40% of area restriction.

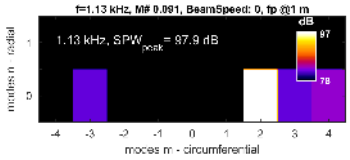

(d) Throttle at 50% of area restriction.

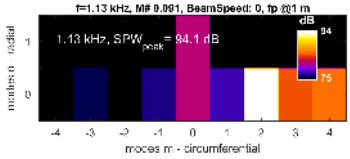

(e) Throttle at 60% of area restriction.

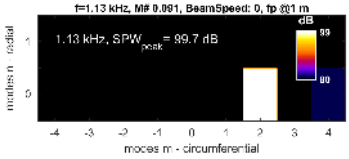

(f) Throttle at 70% of area restriction.

Figure 18. Modal decomposition of the 1st BPF for multiple throttling (RSS = 0.43 and 4250 rpm).

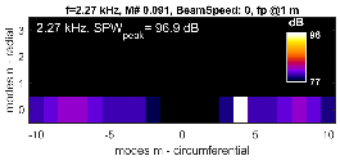

(a) Open throttle.

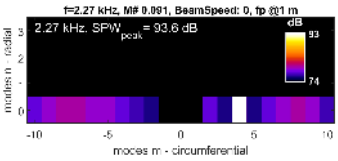

(b) Throttle at 25% of area restriction.

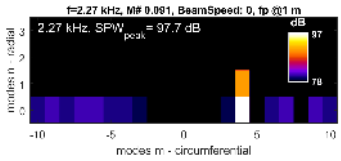

(c) Throttle at 40% of area restriction.

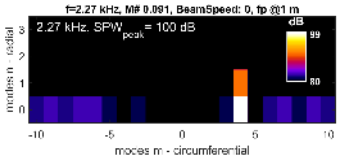

(d) Throttle at 50% of area restriction.

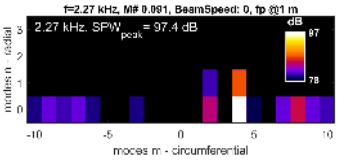

(e) Throttle at 60% of area restriction.

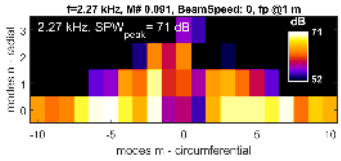

(f) Throttle at 70% of area restriction.

Figure 19. Modal decomposition of the 2nd BPF for multiple throttling (RSS = 0.43 and 4250 rpm).

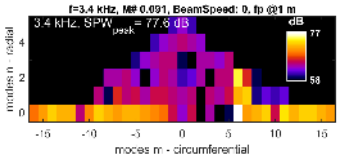

(a) Open throttle.

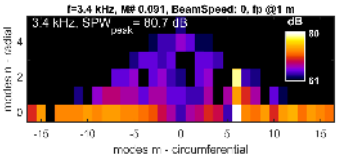

(b) Throttle at 25% of area restriction.

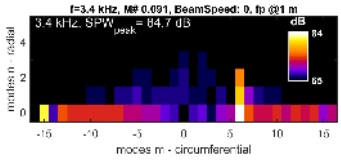

(c) Throttle at 40% of area restriction.

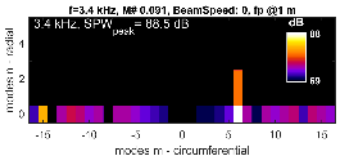

(d) Throttle at 50% of area restriction.

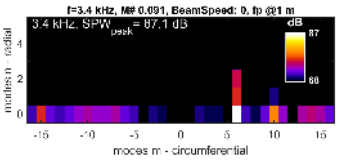

(e) Throttle at 60% of area restriction.

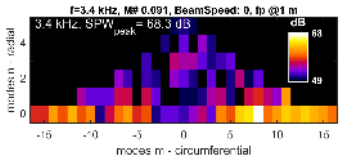

(f) Throttle at 70% of area restriction.

Figure 20. Modal decomposition of the 3rd BPF for multiple throttling (RSS = 0.43 and 4250 rpm).

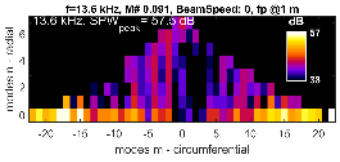

(a) Open throttle.

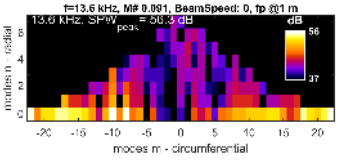

(b) Throttle at 25% of area restriction.

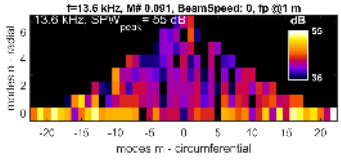

(c) Throttle at 40% of area restriction.

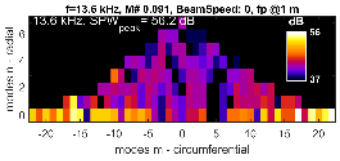

(d) Throttle at 50% of area restriction.

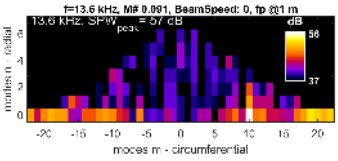

(e) Throttle at 60% of area restriction.

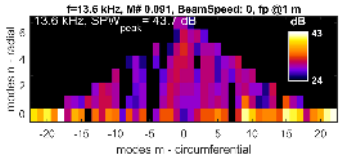

(f) Throttle at 70% of area restriction.

Figure 21. Modal decomposition of the 12th BPF for multiple throttling (RSS = 0.43 and 4250 rpm).

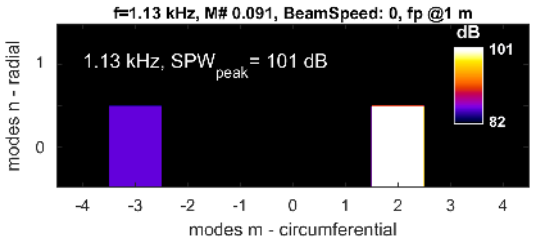

(a) 1st BPF with RSS = 0.41.

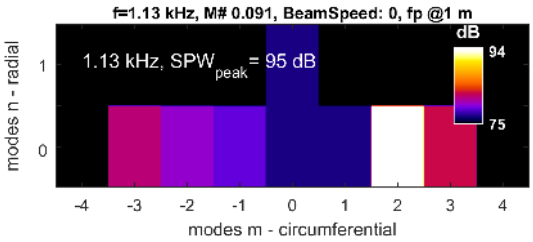

(b) 1st BPF with RSS = 0.95.

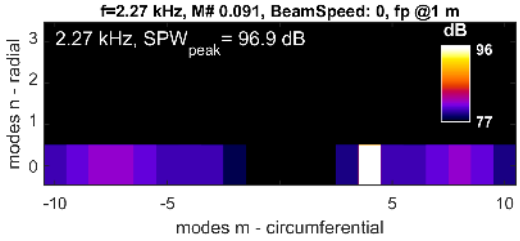

(c) 2nd BPF with RSS = 0.41.

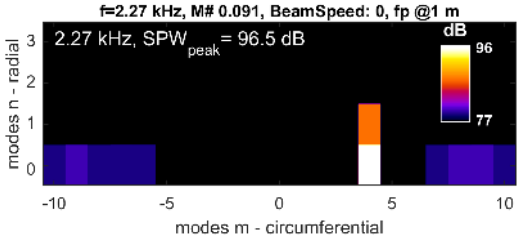

(d) 2nd BPF with RSS = 0.95.

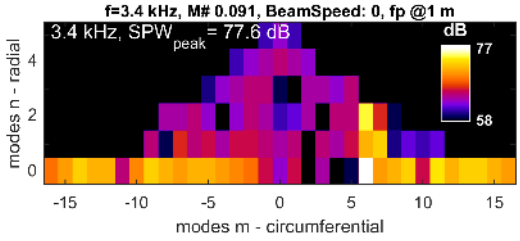

(e) 3rd BPF with RSS = 0.41.

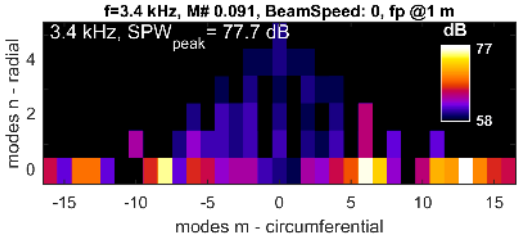

(f) 3rd BPF with RSS = 0.95.

Figure 22. Modal decomposition at fundamental tones for rotor-stator spacings (open throttle and 4250 rpm).

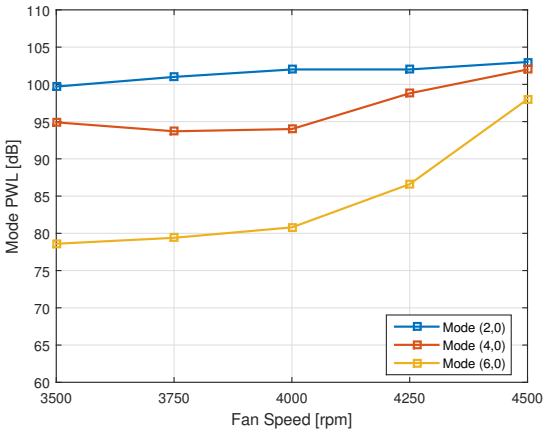

(a) RSS = 0.43.

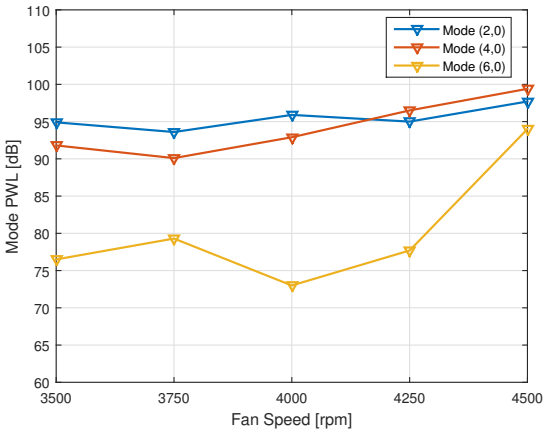

(b) RSS = 0.95.

Figure 23. Interaction modes (2,0), (4,0) and (6,0) compared to fan rotational speed for two rotor-stator spacings (open throttle).

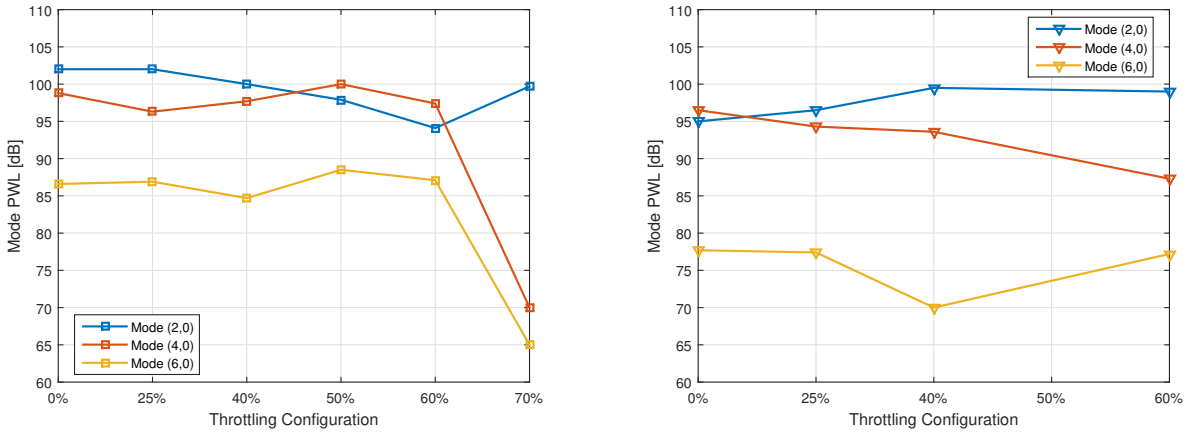

(a) RSS = 0.43. (b) RSS = 0.95.

Figure 24. Interaction modes (2,0), (4,0) and (6,0) compared to throttling configuration for two rotor-stator spacings (4250 rpm).

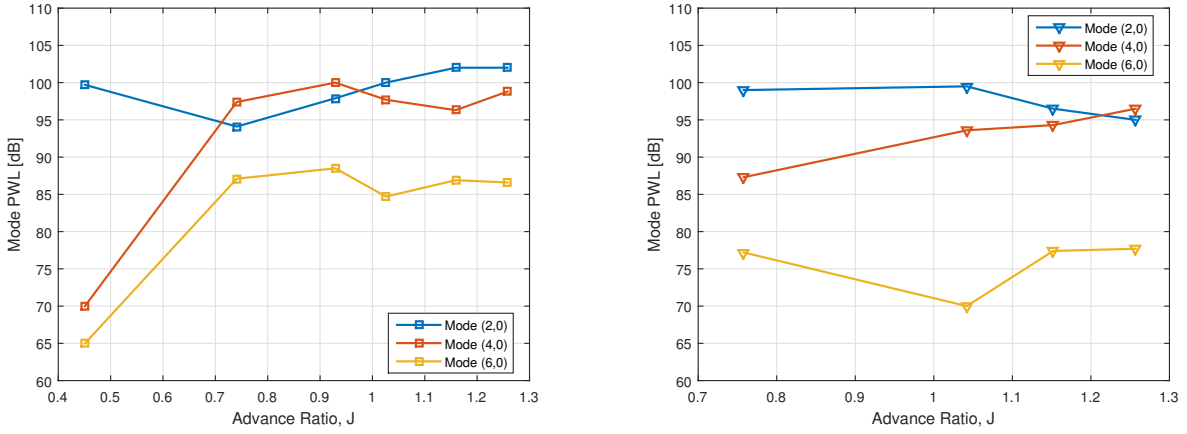

(a) RSS = 0.43. (b) RSS = 0.95.

Figure 25. Interaction modes (2,0), (4,0) and (6,0) compared to advance ratio for two rotor-stator spacings (4250 rpm).

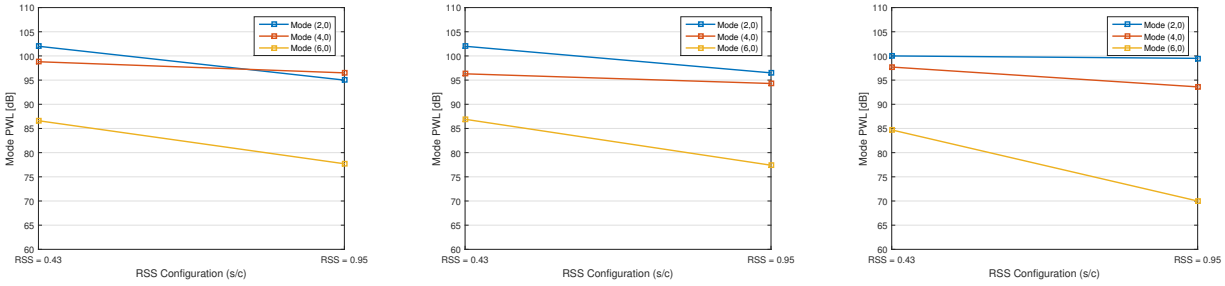

(a) Open throttle. (b) Throttle at 25%. (c) Throttle at 40%.

Figure 26. Interaction modes (2,0), (4,0) and (6,0) compared to rotor-stator spacing for some throttling configurations (4250 rpm).

Table 2. Flow measurements

Condition	RPM	Throt.	ρ [kg/m^3]	M_{inlet}[a]	M_{axial}	M_{tip}	J	α_{hub} [deg]	α_{tip} [deg]	$p_{st,1}$ [Pa]	$p_{st,2}$ [Pa]	$p_{st,3}$ [Pa]	$p_{st,4}$ [Pa]	Reynolds
1	4250	0%	1.052	0.106	0.127	0.343	1.258	17.48	1.28	-511.8	-1325	-721	-557	4.1E+05
2	4250	0%	1.062	0.107	0.128	0.344	1.257	17.50	1.30	-421.5	-1340	-712	-563	4.1E+05
3[b]	4250	0%												
4	4250	25%	1.050	0.098	0.117	0.339	1.159	19.81	2.85	-437.1	-1121	-130	21.7	4.0E+05
5	4250	40%	1.058	0.087	0.104	0.336	1.026	23.27	5.01	-343.8	-909.1	470.1	646.5	4.0E+05
6	4250	50%	1.056	0.079	0.094	0.332	0.929	26.02	6.62	-284.7	-744.7	825	990.5	4.0E+05
7	4250	60%	1.055	0.063	0.075	0.327	0.741	31.96	9.82	-182.4	-485.3	1285	1280	3.9E+05
8	4250	70%	1.055	0.038	0.046	0.322	0.451	42.77	14.94	-67.6	110	1140	1108	3.9E+05
9	4500	0%	1.053	0.113	0.135	0.363	1.260	17.42	1.24	-580	-1496	-845	-639	4.3E+05
10	4000	0%	1.051	0.100	0.120	0.322	1.258	17.48	1.28	-456.2	-1168	-633	-494	3.9E+05
11	3750	0%	1.051	0.093	0.112	0.302	1.255	17.54	1.33	-399.9	-1028	-551	-436	3.6E+05
12	3500	0%	1.051	0.088	0.105	0.282	1.262	17.37	1.21	-348.8	-894	-476	-375	3.4E+05
13	4500	0%	1.063	0.112	0.134	0.364	1.248	17.71	1.44	-470.6	-1503	-792	-636	4.4E+05
14	4000	0%	1.061	0.100	0.120	0.324	1.255	17.55	1.33	-372.8	-1183	-626	-493	3.9E+05
15	3750	0%	1.061	0.093	0.112	0.303	1.250	17.65	1.40	-326.2	-1027	-546	-422	3.6E+05
16	3500	25%	1.060	0.087	0.105	0.283	1.250	17.66	1.41	-285.3	-902	-478	-373	3.4E+05
17	4250	40%	1.059	0.097	0.117	0.340	1.152	20.00	2.97	-356.6	-1131	-153	38.8	4.1E+05
18	4250	60%	1.057	0.088	0.106	0.336	1.042	22.84	4.75	-291.7	-925.9	400.3	619	4.0E+05
19	4250	0%	1.056	0.064	0.077	0.328	0.758	31.39	9.53	-156.5	-504.5	1260	1264	3.9E+05
20[b]	4250	40%												

[a] M_{inlet} refers to the axial speed on the duct before the contraction to the diameter of the fan (0.5 m)
[b] Only spectral analysis of these conditions were performed, due to lack of microphones available on test occasion